

## MIT Open Access Articles

*Toward Industrial Applicability of DNB Predictions  
in CFD With Improved Wall Boiling Models*

The MIT Faculty has made this article openly available. **Please share**  
how this access benefits you. Your story matters.

**Citation:** Feng, Jinyong, Skirpan, Zachary and Baglietto, Emilio. 2020. "Toward Industrial Applicability of DNB Predictions in CFD With Improved Wall Boiling Models." International Conference on Nuclear Engineering, Proceedings, ICONE, 1.

**As Published:** 10.1115/ICONE2020-16080

**Publisher:** American Society of Mechanical Engineers

**Persistent URL:** <https://hdl.handle.net/1721.1/136982>

**Version:** Final published version: final published article, as it appeared in a journal, conference proceedings, or other formally published context

**Terms of Use:** Article is made available in accordance with the publisher's policy and may be subject to US copyright law. Please refer to the publisher's site for terms of use.



## TOWARD INDUSTRIAL APPLICABILITY OF DNB PREDICTIONS IN CFD WITH IMPROVED WALL BOILING MODELS

Jinyong Feng<sup>1</sup>, Zachary Skirpan, Emilio Baglietto  
 Massachusetts Institute of Technology  
 Cambridge, MA

### ABSTRACT

The design of Pressurized Water Reactor (PWR) fuel has to rely on costly prototypical experimental campaigns, due to the inherent limitations of legacy lumped-parameter thermal-hydraulics codes. By resolving the fine spatial scales, computational fluid dynamics (CFD) methods offer the opportunity of delivering improved fuel design, taking full advantage of three-dimensional mixing and turbulence control, but must extend their predictive capabilities to multiphase conditions up to DNB, where the maturity and accuracy of the methods is still developing. In this paper, the closures developed within the Eulerian-Eulerian two-fluid model framework are assembled and extended to a general boiling formulation to deliver prediction of DNB at reactor conditions. The classic heat flux partitioning approach is advanced through selection of optimal closures for interaction length scale, nucleation site density, and bubble departure diameter, and further extended through the addition of a consistent DNB detection criterion, to reflect the near wall two phase characteristics. Assessment is performed at 138 bar against the experimental dataset for vertical pipe, where the inlet subcooling ranges from 1 to 150 K and the mass flux varies from 600 kg/(m<sup>2</sup>.s) to 2650 kg/(m<sup>2</sup>.s). The presented closures demonstrate consistent agreement with the experimental data, in particular in light of the calibration free application, while further work is ongoing to close the remaining gap and support the introduction of further modeling improvements.

Keywords: CFD, multiphase flow, boiling, nucleation site density, bubble departure diameter, DNB

### 1. INTRODUCTION

Subcooled flow boiling has been widely used in many industrial applications and is characterized by large heat transfer

coefficients. In the boiling channel, heat is transferred from the heated wall to the coolant, leading to phase change in the flow. At low and intermediate steam qualities, typical of bubbly flow regimes, nucleate boiling is the dominant heat transfer mechanism. As the steam quality increases, large two phase structures are generated on the heater surface and form a vapor “blanket”, which results in a drastic temperature increase identified as departure from nucleate boiling (DNB). The corresponding heat flux is called critical heat flux (CHF). While CHF can be correlated to the average flow conditions for simple geometries, it strongly depends on the geometrical design of the fuel assemblies, and especially mixing vanes configuration.

Over the past several years, the Thermal-Hydraulics Methods (THM) focus area within the Department of Energy (DOE) supported Consortium for the Advanced Simulation of Light Water Reactors (CASL) program has been developing a methodology to simulate the DNB phenomenon in nuclear reactor cores using computational fluid dynamics (CFD) methods. An understanding of DNB mechanisms and conditions is important to nuclear reactor operation and safety, since DNB results in large and rapid temperature increases that have the potential to degrade the integrity of the fuel rod cladding.

In the past, many empirical correlations for CHF were developed via experimental fitting and applied in 1D and subchannel codes. But these correlations are valid only in the limited specified region of fluid conditions and fluid properties and hold for a certain geometry. The independence on the geometry can only be achieved by the application of CFD methods.

Currently the most conventional CFD approach to model two-phase flows with significant volume fractions of both phases is the Eulerian-Eulerian two-fluid framework of interpenetrating continua. Phase distribution results from solving the phase specific continuity equations for volume fractions, and a separate set of momentum equations is solved for each phase. To simulate the heat transfer in two-phase flow, energy equations are solved.

<sup>1</sup> Contact author: jinyongf@mit.edu

The exchange of mass, momentum and heat between phases are modelled using the corresponding source terms in the conservation equations, thus introducing a few of closures to reflect the physical phenomena, like interfacial forces, nucleation site density, bubble departure diameter, bubble departure frequency, etc.

Leveraging the Eulerian-Eulerian two-fluid framework, the CASL THM team have mainly focused on fuel assembly designs and operating conditions typical of pressurized water reactors (PWRs). In Fiscal Year (FY) 2016 [1], evaluations of baseline boiling closure models were performed with the experimental DNB measurements from a high pressure water system reported by Weatherhead [2]. The experiments were performed at near reactor operating pressure, 138 bar, with varying mass flux and inlet subcooling temperature. The results of the CFD evaluations were compared to CHF measurements and showed that the CFD-predicted CHF values generally followed the qualitative trends for CHF. The relative error between CFD prediction and experimental measurement is within 20%. However, part of the baseline closures was not reflecting the microscopic bubble dynamics features at high pressure. In the meanwhile, the closures were not robust and only 15 test cases out of 105 reported experimental conditions were simulated, which covered the mass flux from 940 kg/(m<sup>2</sup>.s) to 2650 kg/(m<sup>2</sup>.s) and inlet subcooling temperature from 10 K to 100 K.

In parallel to the CASL industrial evaluations in FY17/18, new boiling closure models have been developed and tested by the CASL THM team over the last few years [3-7]. The goal of these newly-developed models has been to improve the accuracy of the predictions so that they can be used by industry in the development of new and modified PWR fuel assemblies.

In this paper, a set of robust and physics-based wall boiling models is proposed for the virtual DNB experiment to realize the goal of simulating the DNB scenarios with the aid of an effective CFD-based DNB prediction methodology. Specific details about the major component of the CASL FY19 boiling models are discussed in Section 2. Section 3 and 4 describe the experiment details and the simulation setup, respectively. Assessment of the closures is discussed in section 5. Finally, the presented work is summarized and a discussion of potential future developments is provided.

## 2. WALL BOILING MODELS

During the past several years, the CASL program has continuously supported the development of advanced interfacial momentum and wall boiling closures that leverage the recent understanding from experimental observation and physics-based analytical derivations. In FY19, the advanced hydrodynamic closures developed within the CASL program have been integrated with a robust set of wall closures for PWR operational pressure and a novel DNB detection criterion, into a robust baseline boiling model, referred to as CASL FY19 boiling model, and its capabilities have been consistently assessed in order to support the adoption of multiphase CFD as virtual DNB

experiment. In this section, detailed descriptions of the boiling closures are discussed.

### 2.1 Wall heat flux partitioning

Multiphase CFD methods resolve the conservation equations for mass, momentum and energy while differing in the approaches and strategies adopted in the physical closure models. The general framework adopted in the present research is the Eulerian-Eulerian two-fluid approach, which assumes that all phases (in our case two fluids) are co-existing inside each computational cell. The volume fraction of the fluids in each cell sums to unity. For each fluid, the full set of conservation equations is solved; therefore, each fluid has a different velocity field. The mechanisms of the interaction between the fluids are the momentum transfer modeled by the interfacial forces, the mass transfer modeled by phase transition and the energy transfer modeled by heat transfer.

The conservation equations for mass, momentum and energy in two-fluid models can be expressed in the following form

$$\begin{array}{l} \text{Mass} \\ \frac{\partial(\alpha_k \rho_k)}{\partial t} + \nabla \cdot (\alpha_k \rho_k \mathbf{u}_k) = \Gamma_k \end{array} \quad (1)$$

$$\begin{array}{l} \text{Momentum} \\ \frac{\partial(\alpha_k \rho_k \mathbf{u}_k)}{\partial t} + \nabla \cdot (\alpha_k \rho_k \mathbf{u}_k \mathbf{u}_k) = -\nabla(\alpha_k p_k) + \nabla \cdot (\alpha_k \boldsymbol{\tau}_k) + \alpha_k \rho_k \mathbf{g} + \mathbf{M}_k^i \end{array} \quad (2)$$

$$\begin{array}{l} \text{Energy} \\ \frac{\partial(\alpha_k \rho_k e_k)}{\partial t} + \nabla \cdot (\alpha_k \rho_k \mathbf{u}_k e_k) = -\nabla(\alpha_k q_k) + \nabla \cdot [(\alpha_k (-p_k + \boldsymbol{\tau}_k) \cdot \mathbf{u}_k) + \alpha_k \rho_k \mathbf{g} \cdot \mathbf{u}_k + \mathbf{E}_k^i] \end{array} \quad (3)$$

where  $\alpha_k$ ,  $\rho_k$ ,  $\mathbf{u}_k$ , and  $e_k$  are the volume fraction, density, velocity, and specific internal energy, respectively, of field- $k$ .  $\Gamma_k$  is the net mass transfer rate of field- $k$ ,  $\boldsymbol{\tau}_k$  is the shear stress,  $\mathbf{M}_k^i$  represents the interfacial momentum forces,  $q_k$  is the local heat flux, and  $\mathbf{E}_k^i$  is the interfacial heat transfer rate, all for field- $k$ .

To simulate the wall boiling phenomena within the Eulerian-Eulerian two-fluid framework, a mechanistic multidimensional model of two-phase flow is required to have models governing local heat transfer and phase change phenomena. The accurate representation of the wall boiling phenomena is extremely important for the multiphase boiling models. The most commonly adopted wall boiling representation relies on the classic heat partitioning concept introduced by Judd and Hwang [8] and adopted by Kurul and Podowski [9], where as shown in Figure 1 and Eq. (4), the total heat flux is computed as the sum of the three partitioned components.

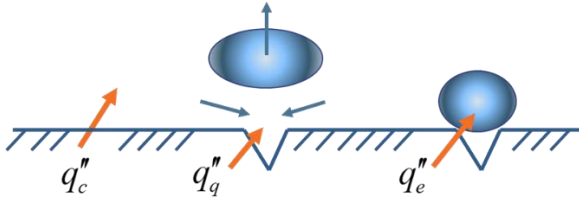


Figure 1: Illustration of the classic RPI's heat partitioning boiling model.

$$q''_{tot} = q''_c + q''_q + q''_e \quad (4)$$

where  $q''_c$ ,  $q''_q$ , and  $q''_e$  represent the heat flux of liquid convective heat transfer, quenching heat transfer and the evaporation, respectively.

As the wall heat flux increases, the generated bubbles accumulate on the wall surface and form a bubbly layer. The accumulation of the bubbly layer can be leveraged to identify the critical heat flux condition at the wall, as departure from nucleate boiling (DNB). Recent study by Demarly [10] found that the microscale hydrodynamics of boiling, essentially bubble microlayer and its dry spot, are the key to the understanding of the boiling crisis, rather the macroscale hydrodynamics. But in order to practically represent the critical transition in CFD, the total heat flux has to be expressed as the sum of the heat transfer from liquid and the convective heat transfer from vapor as given in Eq. (5). A DNB detection criterion is needed to predict the local wall dryout and is discussed next.

$$q''_{tot} = (1 - K_{dry})(q''_{lc} + q''_{lq} + q''_{le}) + K_{dry}q''_{gc} \quad (5)$$

where subscripts  $l$  and  $g$  represent liquid and vapor, respectively.  $K_{dry}$  is the effective wall contact area for vapor. An analytical wall dryout model has been developed and implemented in the recently proposed CASL FY19 closures [11].

Among them, the convection term,  $q''_c$ , represents the convective heat flux which describes the removal of heat by single-phase turbulent convection on the region of the wall that is not affected by boiling.

$$q''_c = h_c(T_w - T_l) = \frac{\rho_l c_{pl} u_l^*}{t_l^+} (T_w - T_l) \quad (6)$$

where  $\rho_l$  is the density of the liquid phase.  $c_{pl}$  is the specific heat of the liquid phase.  $u_l^*$  is the reference velocity from the wall law.  $t_l^+$  is the non-dimensional temperature computed from the wall law.  $T_w$  is the wall temperature.  $T_l$  is the liquid temperature at the center of the cell adjacent to the wall.

The quenching term,  $q''_q$ , describes the enhancement of heat transfer due to the replacement of a departing bubble by an influx of cooler liquid further away from the wall. Quenching heat transfer is the component of heat flux that is used in heating this replacement liquid, as modeled by Del Valle and Kenning [12].

$$q''_q = h_q(T_w - T_q) \quad (7)$$

where  $T_q$  is the temperature of the fresh liquid influx brought to the wall by the departure of a bubble.  $h_q$  is the quenching heat transfer coefficient.

The evaporation term,  $q''_e$ , represents the energy required to produce bubbles from nucleation to departure. The evaporation heat flux is constructed for the following nucleate boiling mechanism: bubbles nucleate and grow on suitably sized cavities on the wall; bubbles reach a critical size, at which point the forces holding the bubble to the wall are no longer balanced. The evaporation heat flux is expressed as

$$q''_e = N'' f \frac{\pi D_d^3}{6} \rho_g h_{lg} \quad (8)$$

where  $h_{lg}$  is the latent heat.  $N''$  is the nucleation site number density.  $f$  is the bubble departure frequency.  $D_d$  is the bubble departure diameter.

In CFD simulation, accurate prediction of the wall boiling phenomena relies on the individual models of bubble departure diameter, bubble departure frequency, nucleation site density, etc. In the meantime, as bubble departures from the wall, its migration behavior are determined by the interfacial momentum forces. Table 1 provides a comprehensive summary of the legacy closures adopted in early CASL activities, and CASL FY19 multiphase boiling models. Substantial efforts have been made to address each of the boiling closures from a physical point of view [11,12]. Due to the page limit, only the discussion of crucial closures, including interaction area density model, bubble departure diameter and nucleation site will be provided in the following sections.

## 2.2 Advanced interaction area density model

The interaction area density, which is related to the inverse of interaction length scale in bubbly flow, is a vital parameter for calculating interfacial momentum transfer, phase transition and local heat transfer in dispersed multiphase flows. In flows where the particles in the dispersed phase are bubbles, for example, the size of the bubbles can change continuously due to breakup and coalescence. The contributions from the evaporation/condensation also change the bubble size.

Kurul-Podowski's interaction length scale model [9,13] has been used in the past which is an empirical correlation that is used in subcooled boiling flows. It is a simple correlation based on the liquid subcooling without the consideration of coalescence and breakup. The coefficients and limiters are tuned from limited experimental data. It cannot predict the bubble distribution on the channel as well as bubble size in the subcooled boiling flows in which multidimensional flow behavior is dominant.

A more general framework to track the particle size distribution can be leveraged from the STAR-CCM+ code, which is the S-gamma models with both one-moment and two-

moment options. The S-gamma is developed and implemented based on the work by Lo and Rao [15], and Lo and Zhang [16]. The S-gamma model adopts the idea of methods of moments (MOM) which was first introduced by Hulburt and Katz [17]. Instead of tracking individual particle groups and introducing transition model between groups, the MOM focuses on the transformation of the problem into lower order of moments of the particle size distribution and tracks the “shape” of the particle size distribution.

For CASL FY19 boiling models, the S-gamma model implemented in STAR-CCM+ is adopted as the interaction area density model with the activation of both coalescence and breakup models. Three modifications are made along with the default parameters. First, the minimum interaction length scale is increased from  $1 \times 10^{-8}$  m to  $1.0 \times 10^{-4}$  m to enforce reasonable

near wall bubble size as observed in the experiment [18]. Another modification is the coalescence coefficient which is increased from 0.01 to 0.2 to account for the very rapid coalescence growth happening at the wall for high pressure conditions. Since the S-gamma model transports the predicted bubble departure diameter from the wall boundary to the bulk, at high pressure, the predicted bubble departure diameter is small which is challenging for the calculation of transport equation and leads to the diminished interaction length scale in the bulk. The last modification is the magnitude of turbulent dispersion force which is increased by a factor of 1.5 to compensate the insufficiency of standard  $k - \varepsilon$  model for turbulent flow prediction. The value of calibration coefficients need further justification with the fuel bundle geometry.

Table 1. Comparison between legacy closures and CASL FY19 boiling model.

Model	Parameters	Legacy closures	CASL FY19 closures
Turbulence model	Turbulence model	Standard $k - \varepsilon$ linear	Standard $k - \varepsilon$ linear
Interaction length scale/density	Interaction length scale	Kurul-Podowski	S-gamma
	Interaction area density	Spherical	Symmetric
Interfacial momentum forces	Drag coefficient	Tomiya (contaminated)	Tomiya (moderate contaminated)
	Lift coefficient	0	Sugrue
	Turbulent dispersion force	Burns	Burns
	Wall lubrication force	N/A	Lubchenko
	Virtual mass force	N/A	N/A
Wall boiling closures	Bubble departure diameter	Tolubinsky and Kostanchuk	Kocamustafaogullari
	Bubble departure frequency	Cole	Zuber
	Active nucleation site density	Lemmert and Chalwa	Li
Bulk boiling/condensation	Condensation-Liquid	Ranz and Marshall	Kim and Park
	Condensation-Vapor	$Nu = 26$	$Nu = 26$
Wall transient conduction	Wall area of bubble influence	Kurul and Podowski	Kurul and Podowski
	Quenching heat transfer coefficient	Del Valle-Kenning	Del Valle-Kenning

## 2.3 Bubble departure diameter closure

The quantification of the bubble departure diameter model plays an important role on the wall boiling model since both evaporation and quenching heat transfer rely on the bubble departure diameter model. The bubble departure diameter model used in the legacy models is the Tolubinsky-Kostanchuk's model [19]. The selection of the Tolubinsky-Kostanchuk approach has been driven in the past by the inconsistencies in the boiling representation, and merely acted as a calibration approach to balance the inaccuracy in the prediction of the nucleation sites density. As shown in Eq. (8), it only correlates the bubble departure diameter with the liquid subcooling, and uses the constants  $D_0 = 0.6$  mm and  $\Delta T_0 = 45$  °C.

$$D_d = D_0 \exp \left[ -\frac{T_{sat} - T_l}{\Delta T_0} \right] \quad (9)$$

A correlation that accounts for the effect of pressure in water-based systems was proposed by Kocamustafaogullari [20]. The correlation relates the bubble departure diameter non-dimensionalized by the capillary length, to a modified term by a density ratio, which makes it useful for a wide range of pressure. Experimental data by Semeria et. al. [21] which measures the bubble departure diameter for pool boiling at pressures as high as 150 bars is used to calibrate the model. The mathematic expression of the model is given as follows

$$d_w = d_1 \theta \left( \frac{\sigma}{g \Delta \rho} \right)^{0.5} \left( \frac{\Delta \rho}{\rho_g} \right)^{0.9} \quad (10)$$

where  $d_1$  is a calibration constant, with a default value of  $1.5126 \times 10^{-3}$  m/radian.  $\theta$  is a wall contact angle for the working fluid, with a default value of 0.722 radians, which is suitable for water systems.  $\sigma$  is the surface tension.

Compared to the Tolubinsky-Kostanchuk' model [19], the new model includes pressure dependence as a critical component to provide a more physical representation of high pressure boiling, and is thus included in the CASL FY19 boiling formulation.

## 2.4 Data-driven nucleation site density closure

The nucleation site density model requires particular attention, as it drives the rapid growth in boiling heat transfer with wall superheat. There are two widely used nucleation site density model, i.e., Lemmert-Chawla' model [22] and Hibiki-Ishii' model [23]. Lemmert-Chawla' active nucleation site density correlation is the most commonly adopted model. However, an important limitation of this model is the lack of dependency on system pressure, which strongly limits its generation applicability.

Hibiki-Ishii' active nucleation site density model provides good predictions over a very wide range of flow conditions and can also account for different boiling surfaces by including a dependence on the contact angle [23]. Studies have been completed to illustrate that the large spread of data on the active nucleation site density can be captured in the nucleation site density models by the inclusion of a dependence on the contact angle of the fluid on the heated material. The Hibiki-Ishii model also depends on the system pressure, which is known to strongly affect the nucleation site density.

At reactor operation pressure, Lemmert-Chawla' model [22] significantly underestimates the nucleation site density. In the meantime, Hibiki-Ishii' model [23] generates better prediction while it experiences steep increases with the wall superheat and the robustness of the model relies on the limiter of superheat temperature.

A data-driven nucleation site density model has been recently developed by Li et al. [24] and preliminarily applied in CFD simulations of subcooled boiling in a vertical heated tube. The new model is based on a parametric analysis of existing experimental data and developed as a function of three crucial parameters relevant to the nucleation site density: wall superheat, system pressure, and contact angle.

$$N_w = N_0(1 - \cos\theta) \exp\{f(P)\} \Delta T_{sup}^{A\Delta T_{sup}+B}, N_0 = 1000 \text{ site/m}^2 \quad (11)$$

where

$$f(P) = 26.006 - 3.678 \exp(-2P) - 21.907 \exp\left(-\frac{P}{24.065}\right)$$

$$A = -0.0002P^2 + 0.0108P + 0.0119$$

$$B = 0.122P + 1.998$$

$$(1 - \cos\theta) = (1 - \cos\theta_0) \left(\frac{T_c - T_{sat}}{T_c - T_0}\right)^Y, \theta_0 = 41.37^\circ, T_c = 374^\circ\text{C}, T_0 = 25^\circ\text{C}.$$

$P$  is the system pressure and in the unit of MPa.

Li et al.' model is applicable in a wide range of pressures: 0.101 MPa~ 19.8 MPa [24]. As shown from Figure 2, the nucleation site density model predicted by Li et al.' model [24]

are in good agreement with the published experimental data [25] compared to the Hibiki-Ishii' model. Another key advantages of Li et al.' model is that there are no artificial limiters of superheat temperature.

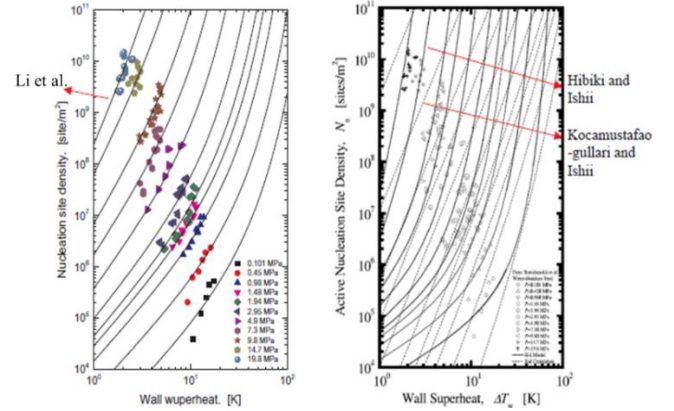


Figure 2: Comparison with Borishanskii et al.'s experiment data [1.38] in different pressures.

## 3. DESCRIPTION OF EXPERIMENT

In the present study, experimental datasets reported by Weatherhead [2] are selected for the assessment of the CASL FY19 closures for two primary reasons. First, the flow boiling condition performed in their experiment is comparable to the realistic PWR operating conditions. Second, the flow boiling test condition and the measured DNB heat flux are explicitly described which are important for nuclear reactor thermal hydraulic safety applications.

A total of 71 experimental conditions are selected for the assessment of the closures. They cover six mass flux groups (673, 913, 1356, 1655, 1980, 2550 kg/(m².s)) and widely varying level of subcooling (1 to 150 K). The experimental setup considers a 7.72 mm inner diameter, type 304 stainless steel vertical tube, 0.4572 m long pipe. Exact number of inlet mass flux and subcooling can be found in the original report of Weatherhead [2].

## 4. NUMERICAL SETUP

All the simulations presented in this paper are performed with the commercial finite volume flow solver, STAR-CCM+, version of 13.02 [26]. CASL FY19 boiling closures are either implicitly implemented in STAR-CCM+ or explicitly implemented through user field functions.

The STAR-CCM+ CFD code employs the finite volume method for its fluid solver, in which the conservation equations are used in their integral form as a starting point. The domain being modeled is divided into a finite number of control volumes (CVs), which is where the conservation equations are applied. The variable values are calculated at the centroid (center) of each CV. The values calculated at the centroid are interpolated to the surfaces of the CV. A suitable quadrature formula is then used to

approximate the surface and volume integrals. The benefit of using a FV method is that it is suitable for complex geometries. STAR-CCM+ typically employs second-order accuracy in time and space.

A segregated flow solver is used, based on the SIMPLE algorithm and is applied on co-located variables using Rhie-Chow interpolation. The simulation of boiling phenomena, especially near the DNB heat flux, introduces considerable challenges on the numerical stability. The wall boiling closures require strong under-relaxation to gradually advect the interface and thermal fields. A set of under-relaxation factors are tested and selected which demonstrates good numerical stability. The volume fraction convection scheme is selected as the first-order upwind scheme. A hybrid Gauss-least square method is used for computing reconstruction gradients, with the Venkatakrishnan's reconstruction gradient limiter. Fluids are simulated with IAPWS-IF97 tables [27].

Since the flow fields are symmetric in the pipe, a quarter of the pipe is simulated to save the computational cost without the loss of physics. Figure 3 shows the boundary conditions of the simulation domain. Fully developed inlet boundary condition is applied on the inlet surface whereas pressure outlet boundary condition is applied on the exit surface. Symmetric boundary conditions are applied on the two side surfaces. Uniform heat flux is applied on the wall surface and unheated regions are placed before and after the heater in order to increase the numerical stability. The total length of the domain is 0.5 m.

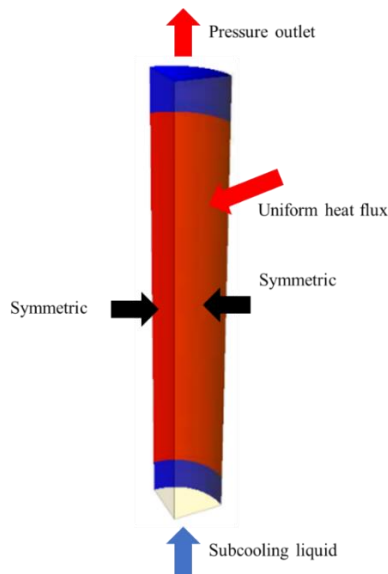


Figure 3: Illustration of the boundary conditions of the simulation domain. Red and blue colors represent the heated and unheated surface, respectively.

The inlet boundary condition is defined using a fully developed pipe flow profile with subcooled temperature. The fully developed inlet velocity distribution is calculated from the following expression:

$$V_{in}(x, y) = \frac{8G}{7\rho_l} \left( \frac{R - \sqrt{x^2 + y^2}}{R} \right)^{\frac{1}{7}} \quad (12)$$

where  $G$  is the inlet mass flux,  $\rho_l$  is the liquid density,  $R$  is the pipe radius. A representative inflow velocity distribution is given in Figure 4. By adopting fully developed inflow profile, the computational cost is reduced.

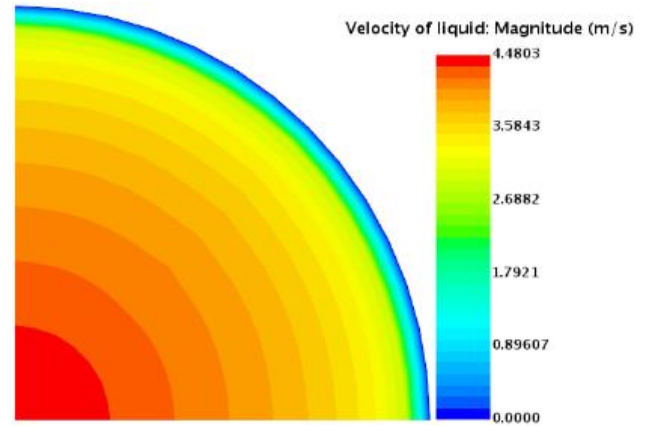


Figure 4: Illustration of the boundary conditions of the simulation domain. Red and blue colors represent the heated and unheated surface, respectively.

A block structured approach is adopted in STAR-CCM+ to generate the mesh for the simulation which allows the user to have precise control of the bulk and near wall mesh resolution. Sensitivity test of the mesh resolution have been performed to deliver a consistent mesh configuration. As shown in Figure 5, structured mesh configuration is obtained on the cross-section and the aspect ratio between the transverse and streamwise direction is around 2.5. Since the flow development along the pipe is mild, affordable computational cost is possible by adopting higher aspect ratio without losing physical representation of the physics. The number of total cells is 0.14 million and the values of wall  $y^+$  ranges from 37.8 to 190.8 based on the inlet mass flux.

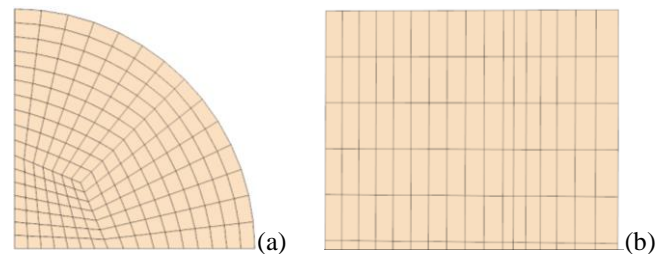


Figure 5: Cross-sectional and front view of the mesh configuration.

## 5. RESULTS AND DISCUSSION

Assessment of the CASL FY19 closures is performed for all the 71 experimental conditions within the range of subcooling

and mass fluxes of interests. Both qualitative and quantitative analysis are discussed in this section.

## 5.1 Boiling curve

Step-increased heat flux is uniformly applied on the wall boundary with increments of  $0.05 \text{ MW/m}^2$  every 5000 iterations. By iterating in this manner, boiling curves are generated and a representative boiling curve is given in Figure 6 where the CHF is characterized by an abrupt increase in wall temperature. The experimental condition corresponding to the boiling curve in Figure 6 is inlet subcooling of  $86.4 \text{ K}$  and mass flux of  $1681.7 \text{ kg/(m}^2\cdot\text{s)}$ . As shown in Figure 6, the slope of the wall temperature represents three modes of heat transfer: single phase heat transfer, nucleate boiling heat transfer and DNB. Figure 7 and Figure 8 compare the boiling curves for different combinations of mass fluxes and inlet subcooling. As expected, higher mass flux and inlet subcooling delay the occurrence of DNB, thus having higher CHF. DNB is detected as the point where the wall superheat jumps tremendously and the temperature increment is more than  $10 \text{ K}$ .

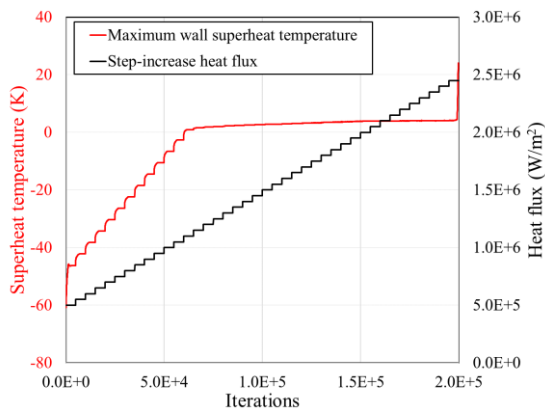


Figure 6: Evolution of wall superheat temperature versus the step-increased heat flux. Representative case has inlet subcooling of  $86.4 \text{ K}$  and mass flux of  $1681.7 \text{ kg/(m}^2\cdot\text{s)}$ .

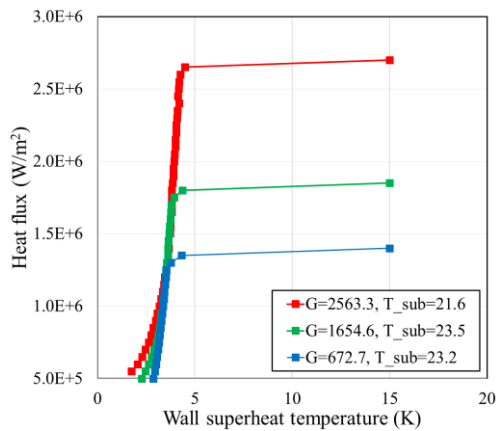


Figure 7: Boiling curves for different mass fluxes with comparable inlet subcooling.

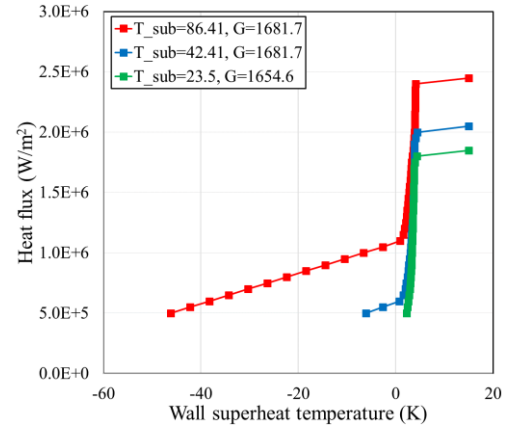


Figure 8: Boiling curves for different inlet subcooling with comparable inlet mass flux.

## 5.2 Temperature and void fraction distributions

Weatherhead's experiment provide precious measurement of inlet subcooling, mass fluxes and CHF. Unfortunately, three-dimensional distributions of the void fraction and temperature are not reported due to the limitations of experimental techniques at that time. By resolving the flow fields on a sufficiently fine spatial scale, CFD simulations can complement the physical experiment by providing additional flow information from numerical measurement planes as shown in Figure 9. Void fraction and temperature distributions along the streamwise direction and on the cross section at the end of heater are given in Figure 10 and Figure 11. Subcooling liquid enters the pipe and reaches saturation on the heater surface. Significant amount of void are generated on the heated surface and switch the mode of nucleate boiling heat transfer to convective heat transfer by vapor. The temperature and void fraction distributions from a representative flow condition (inlet subcooling of  $23.21 \text{ K}$  and mass flux of  $695.17 \text{ kg/(m}^2\cdot\text{s)}$ ) are reasonable and meet the expectations.

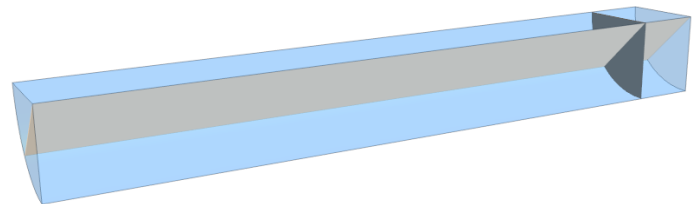


Figure 9: Illustration of the numerical measurement planes (grey color) for void fraction and temperature distributions.

Figure 10: Superheat and void fraction distributions along the streamwise direction.

Figure 11: Cross-sectional view of the superheat and void fraction distributions at the end of the heater.

### 5.3 Critical heat flux

Figure 12 compares the CHF from CFD simulations and the CHF measured from experiment across the entire datasets. The

root-mean-square error of the CFD simulations is 12.5% which indicates that the CASL FY19 closures generate acceptable prediction on the CHF.

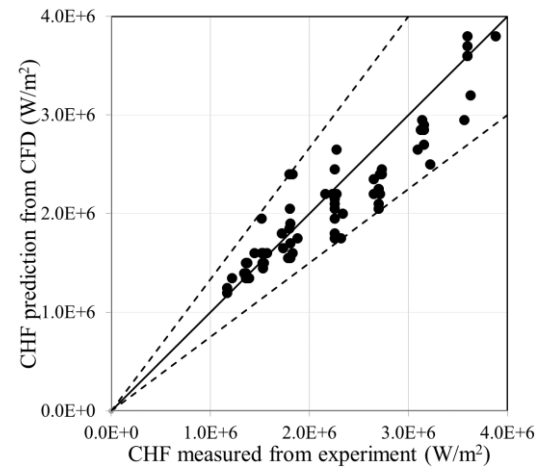
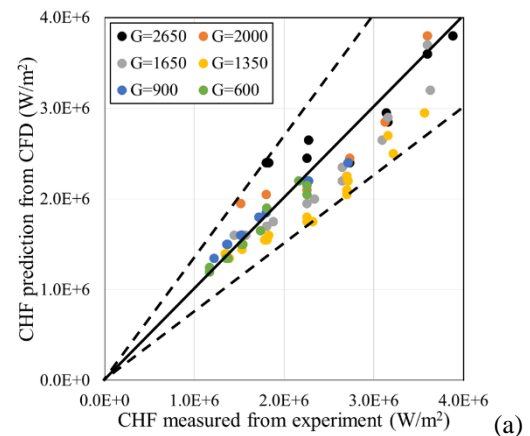


Figure 12: Comparison between CHF prediction from CFD and CHF measured from experiment where the dash lines represent  $\pm 25\%$  relative error.

All the experiments are conducted with the identical geometry and system pressure while the inflow subcooling and mass fluxes are intentionally different to build a wide range of database. Experimental conditions are classified into separate groups based on inlet subcooling and mass fluxes in order to identify the applicability and limitations of the CASL FY19 closures. Figure 13 compares the relative error for six distinct groups of mass fluxes. It is observed that the relative differences between the experiment and CFD simulations are within 15%. No apparent dependence is found between mass fluxes and CHF predictions which supports that the CHF predictions for the presented geometry can be achievable with one set of mesh configuration even though the near wall  $y^+$  ranges from 37.8 to 190.8 for different mass fluxes.



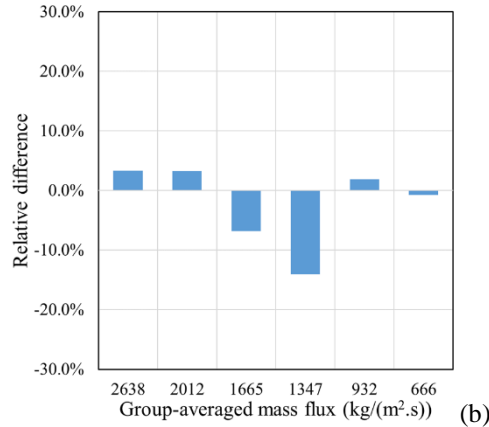


Figure 13: Comparison between CHF prediction from CFD and CHF measured from experiment for different groups of mass fluxes.

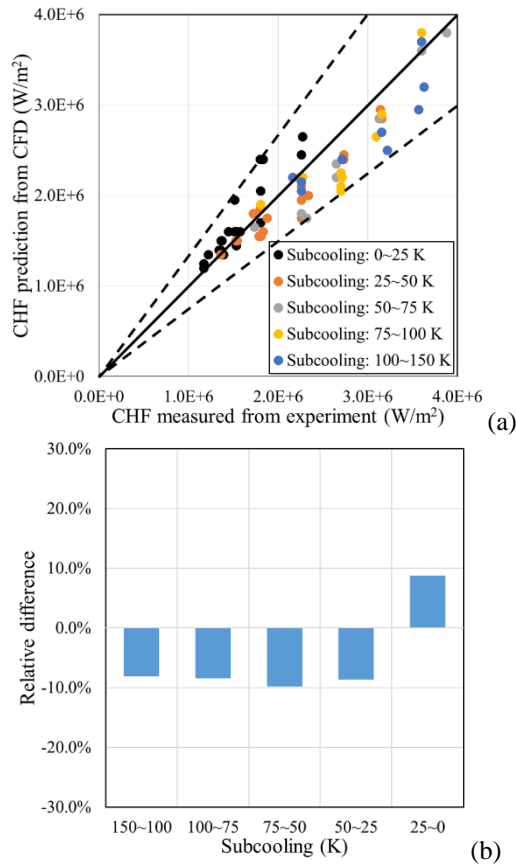


Figure 14: Comparison between CHF prediction from CFD and CHF measured from experiment for different subcooling.

Figure 14 compares the relative error for five different groups of inlet subcooling. It is observed that the CASL FY19 closures overpredict the CHF for low subcooling and underestimate the CHF for high subcooling. Since Kim-Park's condensation model [7] is derived and validated at system pressure of 1 bar, extending the application of their closure to significantly higher system pressure introduces inaccurate

representation of the physics during the boiling process. Although the relative error for each inlet subcooling group is within 10%, additional research is required to improve the understanding of the evaporation/condensation process at reactor operating pressure.

## 6. CONCLUSION

In this paper, a set of improved physics-based momentum closures developed in the context of the CASL program has been coupled to an optimized implementation of the classic RPI heat partitioning model to support accurate prediction of DNB at prototypical PWR conditions. Substantial efforts have been placed on improving the accuracy of each closure from a physical point of view and then the integrated model is assembled and tested with the ANL-Weatherhead experimental database. Selected experimental database has comparable reactor operating pressure and explicit reports of inlet boundary conditions and CHF.

Both qualitative and quantitative comparisons are performed across six mass flux groups (600, 930, 1350, 1650, 2000, 2650 kg/(m².s)) and wide range of inlet subcooling (1 to 150 K). The root-mean-square error of all the investigated condition is 12.5%. By separating the entire datasets into different groups of mass flux and inlet subcooling, it is observed that the accuracy of the CASL FY19 closures depends on the subcooling while the maximum relative error for each group is within 10%. Boiling curves, void fraction and temperature distributions are also analyzed and demonstrate consistent physical predictions of the wall boiling phenomena at reactor conditions. The CFD results provide a valuable complement to the high fidelity experimental measurement.

The presented research demonstrates the potential of numerically simulating DNB phenomena using physics-based framework and advanced closures. Future work will focus both on the assessment of the current closures on industrial 5x5 mixing vanes applications and further on the extension of the model by incorporated more advanced description of the wall heat partitioning, which have been produced as part of the CASL effort.

## ACKNOWLEDGEMENTS

The authors gratefully appreciate the support of the Consortium for Advanced Simulation of Light Water Reactors (CASL) program. The authors would like to acknowledge the prior contributions from SeungJun Kim, at LANL, on the assessment of the closures.

## REFERENCES

- [1] S. J. Kim, E. Baglietto, B. Okhuysen, and E. Demarly, "CFD study of a multi-phase subcooled flow boiling model and the evaluation of the model's predictive capability for boiling characteristics," *Proceedings of NUTHOS-II*, 2016.
- [2] R. Weatherhead, "Nucleate boiling characteristics and the

- critical heat flux occurrence in subcooled axial-flow water systems,” 1963.
- [3] N. Lubchenko, B. Magolan, R. Sugrue, and E. Baglietto, “A more fundamental wall lubrication force from turbulent dispersion regularization for multiphase CFD applications,” *Int. J. Multiph. Flow*, vol. 98, pp. 36–44, 2018.
  - [4] R. M. Sugrue, “A robust momentum closure approach for multiphase computational fluid dynamics applications,” *Ph.D. Thesis*, Massachusetts Institute of Technology, 2017.
  - [5] J. Feng and I. A. Bolotnov, “Evaluation of bubble-induced turbulence using direct numerical simulation,” *Int. J. Multiph. Flow*, vol. 93, pp. 92–107, 2017.
  - [6] J. Feng and I. A. Bolotnov, “Interfacial force study on a single bubble in laminar and turbulent flows,” *Nucl. Eng. Des.*, vol. 313, pp. 345–360, 2017.
  - [7] S.-J. Kim and G.-C. Park, “Interfacial heat transfer of condensing bubble in subcooled boiling flow at low pressure,” *Int. J. Heat Mass Transf.*, vol. 54, no. 13–14, pp. 2962–2974, 2011.
  - [8] R. L. Judd and K. S. Hwang, “A comprehensive model for nucleate pool boiling heat transfer including microlayer evaporation,” *ASME J. Heat Transf.*, vol. 98, no. 4, pp. 623–629, 1976.
  - [9] N. Kurul and M. Z. Podowski, “Multidimensional effects in forced convection subcooled boiling,” in *Proceedings of the Ninth International Heat Transfer Conference*, 1990, vol. 2, pp. 19–24.
  - [10] E. Demarly, “A new approach to predicting Departure from Nucleate Boiling (DNB) from direct representation of boiling heat transfer physics,” *Ph.D. Thesis*, Massachusetts Institute of Technology, 2020.
  - [11] J. Feng, R. Kommajosyula, and E. Baglietto, “Finalize CASL Closure Models with Wall Model Improvements including Nucleation Site Density and Bubble Departure diameter,” *CASL Milestone L2:THM.DNB.P19.02*, 2019.
  - [12] V. H. Del Valle and D. B. R. Kenning, “Subcooled flow boiling at high heat flux,” *Int. J. Heat Mass Transf.*, vol. 28, no. 10, pp. 1907–1920, 1985.
  - [13] R. Brewster, J. Feng, and E. Baglietto, “Industry Application of CASL DNB Methods,” *CASL Milestone L2:THM.DNB.P19.01*, 2019.
  - [14] N. Kurul and M. Z. Podowski, “On the modeling of multidimensional effects in boiling channels,” in *Proceedings of the 27th national heat transfer conference*, 1991, pp. 301–314.
  - [15] S. Lo and P. Rao, “Modelling of droplet breakup and coalescence in an oil-water pipeline,” in *6th International Conference on Multiphase Flow, ICMF*, 2007, pp. 9–13.
  - [16] S. Lo and D. Zhang, “Modelling of break-up and coalescence in bubbly two-phase flows,” *J. Comput. Multiph. Flows*, vol. 1, no. 1, pp. 23–38, 2009.
  - [17] H. M. Hulburt and S. Katz, “Some problems in particle technology: A statistical mechanical formulation,” *Chem. Eng. Sci.*, vol. 19, no. 8, pp. 555–574, 1964.
  - [18] J. Garnier, E. Manon, and G. Cubizolles, “Local measurements on flow boiling of refrigerant 12 in a vertical tube,” *Multiph. Sci. Technol.*, vol. 13, no. 1–2, pp. 1–111, 2001.
  - [19] V. I. Tolubinsky and D. M. Kostanchuk, “Vapour bubbles growth rate and heat transfer intensity at subcooled water boiling,” in *International Heat Transfer Conference 4*, 1970, vol. 23.
  - [20] G. Kocamustafaogullari, “Pressure dependence of bubble departure diameter for water,” *Int. Commun. Heat Mass Transf.*, vol. 10, no. 6, pp. 501–509, 1983.
  - [21] H. Semeria, “No Title,” *J. L’Hydraulique la Société. Hydrotechnique Fr.*, 1962.
  - [22] M. Lemmert and J. M. Chawla, “Influence of flow velocity on surface boiling heat transfer coefficient,” *Heat Transf. Boil.*, vol. 237, p. 247, 1977.
  - [23] T. Hibiki and M. Ishii, “Active nucleation site density in boiling systems,” *Int. J. Heat Mass Transf.*, vol. 46, no. 14, pp. 2587–2601, 2003.
  - [24] Q. Li *et al.*, “Development, verification and application of a new model for active nucleation site density in boiling systems,” *Nucl. Eng. Des.*, vol. 328, pp. 1–9, 2018.
  - [25] V. M. Borishanskii, G. I. Bobrovich, and F. P. Minchenko, “Heat transfer from a tube to water and to ethanol in nucleate pool boiling,” in *Problems of Heat Transfer and Hydraulics of Two-Phase Media*, Elsevier, 1969, pp. 85–106.
  - [26] “STAR-CCM+, version 13.02,” 2018.
  - [27] “IAPWS Industrial Formulation 1997 for the Thermodynamic Properties of Water and Steam,” in *International Steam Tables*, Berlin, Heidelberg: Springer Berlin Heidelberg, 2008, pp. 7–150.